Disordered magnetic multilayers: Electron transport within the coherent potential approximation

K. Carva,[1,*] I. Turek,[2] J. Kudrnovský,[3] and O. Bengone[4]
[1]*Faculty of Mathematics and Physics, Department of Electronic Structures, Charles University, Ke Karlovu 5, CZ-12116 Prague 2, Czech Republic*
[2]*Institute of Physics of Materials, Academy of Sciences of the Czech Republic, Žižkova 22, CZ-61662 Brno, Czech Republic*
[3]*Institute of Physics, Academy of Sciences of the Czech Republic, Na Slovance 2, CZ-18221 Prague 8, Czech Republic*
[4]*Institut de Physique et Chimie des Matériaux de Strasbourg, UMR 7504 ULP-CNRS, 23 rue du Loess, Boîte Postale 43, F-67034 Strasbourg Cedex 2, France*
(Received 3 February 2006; published 19 April 2006)

We develop an efficient technique for *ab initio* calculations of the current-perpendicular-to-plane (CPP) electron transport in disordered magnetic multilayers. The method is based on the tight-binding linear muffin-tin orbital theory and the coherent potential approximation (CPA) to treat the substitutional randomness in an effective-medium approach. A formulation of the CPA vertex corrections, giving rise to an incoherent part of the CPP conductance, is described in detail and the numerical implementation is discussed. The developed approach is illustrated on several disordered systems derived from fcc Co-Cu-Co trilayers and its results are compared to those of a supercell technique simulating the randomness in terms of two-dimensional lateral supercells. The overall good agreement of the two techniques proves reliability of the CPA for a number of specific features encountered in disordered multilayers. As another example, results for layered diluted ferromagnetic (Ga, Mn)As semiconductors are reported, including a brief discussion of spin-resolved and incoherent CPP conductances and a comparison to bulk residual resistivities.

DOI: 10.1103/PhysRevB.73.144421 PACS number(s): 72.10.Fk, 72.15.Gd, 72.25.Mk

I. INTRODUCTION

The phenomenon of giant magnetoresistance (GMR) has already served as a basis for many important applications, although only a decade and one-half passed since its discovery.[1,2] It raised interest in spin-dependent electron transport in mesoscopic systems, in particular in the current-perpendicular-to-planes (CPP) geometry of epitaxial metallic magnetic multilayers.[3–6] Magnetic tunnel junctions represent another fast developing branch of the CPP transport.[4] On the theoretical side, a number of theoretical approaches have been proposed addressing various aspects of these topics. Most of them employ the Landauer formalism for a central region of a finite thickness coupled to semi-infinite leads.[7] At present, all standard techniques of *ab initio* electronic structure calculations can be routinely used for a parameter-free description of the CPP transport in magnetic multilayers. These approaches employ the linearized augmented plane waves (LAPW),[8,9] the tight-binding (TB) linear muffin-tin-orbital (LMTO) method,[10–12] or the Korringa-Kohn-Rostoker (KKR) method in its screened (SKKR)[13,14] and layer (LKKR)[15] versions.

The majority of applications of the above techniques refer to multilayers with chemically pure layers and perfect (abrupt) interfaces, i.e., to the ballistic regime. The case of disorder at interfaces and/or inside the layers—often encountered in real samples—represents additional obstacle for theoretical treatments on an *ab initio* level. Existing successful solutions to this problem employ a technique of two-dimensional (2D) supercells (SC).[10–12,16] An obvious alternative, namely the systematic application of the coherent potential approximation (CPA),[17–19] has been used only exceptionally for the layered systems, being confined mostly to models with a single orbital per site[20] or to a weak scattering limit.[21] This situation contrasts the residual resistivity of random bulk alloys within the Kubo linear response theory,[22] where the general CPA formulation[23] was implemented in the *ab initio* KKR method a long time ago[24] and has been used by a number of authors[25–27] whereas brute force approaches are rather rare.[28] Recently, a LMTO-CPA technique for electron transport in bulk random alloys has been developed as well.[29,30]

The disorder effects on transport properties of magnetic multilayers are non-negligible, ranging from modifications of effective potential barriers at the interfaces over non-conservation of the $\mathbf{k}_{\parallel}$ vector in the scattering process to changes (either decrease or increase) of the conductance, depending on the particular system and the spin channel.[10,11] The randomness inside thick layers is responsible for a crossover from the ballistic to the ohmic (diffusive) regime,[12] accompanied in some cases by a change of sign of the GMR effect.[31,32] All these phenomena become important especially for intrinsically disordered systems, such as permalloy (Ni-rich fcc NiFe alloys)[4,6] and diluted magnetic semiconductors (e.g., Mn-doped GaAs),[33–35] that are materials for applications in spintronics.

The present paper aims at a development of an efficient scheme for the CPP transport properties of substitutionally disordered epitaxial multilayers within an *ab initio* TB-LMTO-CPA framework. The main effort is focused on a formulation and a numerical implementation of the so-called vertex corrections arising in configuration averaging of a product of two Green's functions.[23] As it is well known, their proper inclusion is inevitable for an approximate, but consistent theory that guarantees basic laws of particle and energy conservation; the CPA represents a consistent theory from this point of view.[23] In addition to the first results obtained within the CPA, a comparison to previous results of a SC

technique is presented as well. The paper is organized as follows: The theoretical formulation of the CPP transport problem for disordered multilayers is contained in Sec. II with a general solution of the LMTO-CPA vertex corrections sketched in the Appendix. Section III describes the numerical implementation and other calculational details while the Sec. IV presents the results for several selected magnetic multilayers. Conclusions are summarized in Sec. V.

II. FORMALISM

A. Description of the systems

The epitaxial magnetic multilayers considered in this paper consist of nonrandom semi-infinite left ($\mathcal{L}$) and right ($\mathcal{R}$) leads attached to a central (intermediate) region containing an arbitrary sequence of magnetic and nonmagnetic layers with possible substitutional disorder at the interfaces and/or inside the layers. We neglect random lattice relaxations due to random occupations of individual lattice sites, i.e., all configurations of the disordered intermediate region have the same nonrandom geometric structure. The latter however can be different from that of the leads and also local structural variations along the direction perpendicular to the atomic layers, e.g., the layer relaxations, can be included; the basic assumption is the perfect 2D periodicity of the nonrandom structure in directions parallel to the atomic layers. The same 2D translational invariance of the configurationally averaged physical system is assumed as well.

For simplicity, the developed formalism is confined to multilayers with collinear magnetic structures and with neglected spin-orbit effects. As a consequence, the CPP conductances can be evaluated separately in the two spin channels (a two-current model); for this reason the spin index σ ($\sigma=\uparrow,\downarrow$) is omitted in Secs. II B and II C as well as in the Appendix.

B. Electronic structure

The one-particle electronic structure of each random configuration of the multilayer can be described within the TB-LMTO method in the atomic-sphere approximation (ASA)[36–38] in terms of energy-independent TB structure constants $S^{LL'}_{\mathbf{RR}'}$ and energy-dependent potential functions $P_{\mathbf{R}L}(z)=P_{\mathbf{R}\ell}(z)$, both chosen here in the TB-representation of the LMTO theory. The indices $\mathbf{R}$, $\mathbf{R}'$ label the lattice sites, the indices L, L' denote usual combinations of orbital and magnetic quantum numbers, $L\equiv(\ell,m)$, and z denotes a complex energy variable. The structure constant matrix S with elements $S^{LL'}_{\mathbf{RR}'}$ describes mutual positions of the lattice sites while the scattering properties of the (spherically symmetric) one-electron potentials inside all atomic spheres are contained in a site-diagonal matrix of potential functions $P(z)$ with elements $P^{LL'}_{\mathbf{RR}'}(z)=\delta_{\mathbf{RR}'}\delta_{LL'}P_{\mathbf{R}L}(z)$. The central quantity for the one-particle Green's function[37–39] (GF) (resolvent of the one-electron ASA Hamiltonian) is an auxiliary GF matrix $g(z)$ with elements $g^{LL'}_{\mathbf{RR}'}(z)$ defined by

$$g(z)=[P(z)-S]^{-1}. \tag{1}$$

Substitutional disorder in the present model assumes random occupation of selected sites of the intermediate region by several atomic species $Q=A,B,\ldots$. The occupations of two different sites $\mathbf{R}\neq\mathbf{R}'$ are completely uncorrelated; the probability of a particular configuration is thus fully specified by site-dependent concentrations $c^Q_{\mathbf{R}}$ of the species Q (with an obvious sum rule $\Sigma_Q c^Q_{\mathbf{R}}=1$). The configuration average of a number of one-particle properties within the CPA[37,38,40] can be reduced to the averaged auxiliary GF matrix, $\langle g(z)\rangle\equiv\bar{g}(z)$, given explicitly by

$$\bar{g}(z)=[\mathcal{P}(z)-S]^{-1}, \tag{2}$$

where $\mathcal{P}(z)$ denotes a nonrandom site-diagonal matrix of the coherent potential functions $\mathcal{P}^{LL'}_{\mathbf{R}}(z)$ that define an effective CPA medium. The latter quantities are chosen to satisfy the CPA self-consistency conditions

$$\langle t_{\mathbf{R}}(z)\rangle\equiv\sum_Q c^Q_{\mathbf{R}}t^Q_{\mathbf{R}}(z)=0, \tag{3}$$

where $t^Q_{\mathbf{R}}(z)$ denotes the single-site T-matrix with matrix elements $t^{Q;LL'}_{\mathbf{R}}(z)$ that describes the scattering from a Q impurity at the $\mathbf{R}$th site with respect to the effective CPA medium. An explicit expression for $t^Q_{\mathbf{R}}(z)$ (with orbital indices omitted) is

$$t^Q_{\mathbf{R}}(z)=\{1+[P^Q_{\mathbf{R}}(z)-\mathcal{P}_{\mathbf{R}}(z)]\bar{g}_{\mathbf{RR}}(z)\}^{-1}[P^Q_{\mathbf{R}}(z)-\mathcal{P}_{\mathbf{R}}(z)], \tag{4}$$

where $P^Q_{\mathbf{R}}(z)$ denote matrices of site- and species-resolved potential functions. More details on the CPA, especially for layered systems, can be found in Refs. 37 and 38.

C. CPP transport

The zero-temperature CPP conductance of the disordered multilayer (in one spin channel) per unit 2D cell is within the Kubo-Landauer approach[7] and the TB-LMTO formalism[10,29] given as

$$C=\frac{e^2}{h}\frac{1}{N_\parallel}\mathrm{Tr}\langle g(a)\mathcal{B}_{\mathcal{L}}g(b)\mathcal{B}_{\mathcal{R}}\rangle, \tag{5}$$

where $N_\parallel$ refers to a large number of 2D cells in directions parallel to atomic layers and the trace is taken over the site and orbital indices of the intermediate region. The complex energy arguments of the GF matrices in Eq. (5) are related to the system Fermi energy E_F by infinitesimal shifts, namely $a=E_F+i\eta$, $b=E_F-i\eta$, where $\eta\to 0^+$. The nonrandom matrices $\mathcal{B}_{\mathcal{L}}$ and $\mathcal{B}_{\mathcal{R}}$ are related to anti-Hermitean parts of the self-energies of the semi-infinite leads. In a principal-layer technique,[37,38] the lattice sites are denoted as pairs $\mathbf{R}\equiv(p,\mathbf{S})$ where p is the integer principal-layer index and $\mathbf{S}$ labels the lattice sites of one principal layer. The intermediate region consists of N principal layers with index bounded by $1\leqslant p\leqslant N$, while the left and right leads correspond to $p\leqslant 0$ and $p\geqslant N+1$, respectively. The necessary condition for applicability of the pricipal-layer formalism is vanishing of elements of the TB structure constant matrix $S^{LL'}_{\mathbf{RR}'}$ for lattice

sites not belonging to the same or neighboring principal layers, i.e., $S^{LL'}_{p\mathbf{S},p'\mathbf{S}'}=0$ for $|p-p'|>1$. Employing this notation, the matrices $\mathcal{B}_{\mathcal{L}}$ and $\mathcal{B}_{\mathcal{R}}$ are explicitly expressed as

$$(\mathcal{B}_{\mathcal{L}})^{LL'}_{p\mathbf{S},p'\mathbf{S}'} = i\delta_{p1}\delta_{p'1}\sum_{\mathbf{S}_1L_1}\sum_{\mathbf{S}_2L_2} S^{LL_1}_{1\mathbf{S},0\mathbf{S}_1}[\mathcal{G}_{\mathcal{L}}(a)-\mathcal{G}_{\mathcal{L}}(b)]^{L_1L_2}_{\mathbf{S}_1\mathbf{S}_2}S^{L_2L'}_{0\mathbf{S}_2,1\mathbf{S}'},$$

$$(\mathcal{B}_{\mathcal{R}})^{LL'}_{p\mathbf{S},p'\mathbf{S}'} = i\delta_{pN}\delta_{p'N}\sum_{\mathbf{S}_1L_1}\sum_{\mathbf{S}_2L_2} S^{LL_1}_{N\mathbf{S},(N+1)\mathbf{S}_1}[\mathcal{G}_{\mathcal{R}}(a) - \mathcal{G}_{\mathcal{R}}(b)]^{L_1L_2}_{\mathbf{S}_1\mathbf{S}_2}S^{L_2L'}_{(N+1)\mathbf{S}_2,N\mathbf{S}'}, \quad (6)$$

where $\mathcal{G}_{\mathcal{L}}(z)$ and $\mathcal{G}_{\mathcal{R}}(z)$ denote the surface GF's of the two semi-infinite leads.[41] Note that the matrices $\mathcal{B}_{\mathcal{L}}$ and $\mathcal{B}_{\mathcal{R}}$ are localized to the first and the Nth principal layer, respectively.

The configurational average of conductance, Eq. (5), is more complicated than that of one-particle properties, essentially because $\langle g(a)\otimes g(b)\rangle$ differs from $\langle g(a)\rangle\otimes\langle g(b)\rangle$ by the vertex corrections (VC). The original formulation of the VC compatible with the CPA average of one-particle GF's and a proof of their analytical properties including the Ward identity was given in Ref. 23. In the Appendix, the basic formulas for VC are rewritten in the present LMTO-CPA formalism and a final expression for quantities encountered in transport studies is derived.

The resulting formula for the conductance, Eq. (5), can be separated in two contributions: the coherent (ballistic, specular) part C_{coh} and the incoherent (diffusive, vertex) part C_{VC}, see Eq. (A14):

$$C = C_{\mathrm{coh}} + C_{\mathrm{VC}}, \quad (7)$$

where

$$C_{\mathrm{coh}} = \frac{e^2}{h}\frac{1}{N_{\parallel}}\mathrm{Tr}\{\bar{g}(a)\mathcal{B}_{\mathcal{L}}\bar{g}(b)\mathcal{B}_{\mathcal{R}}\} \quad (8)$$

and

$$C_{\mathrm{VC}} = \frac{e^2}{h}\frac{1}{N_{\parallel}}\mathrm{Tr}\langle g(a)\mathcal{B}_{\mathcal{L}}g(b)\mathcal{B}_{\mathcal{R}}\rangle_{\mathrm{VC}}. \quad (9)$$

Since the leads and the configurationally averaged system exhibit the 2D translational invariance, the 2D lattice Fourier transform is used to perform the matrix multiplications in Eqs. (6) and (8). For this purpose, the lattice sites are denoted as $\mathbf{R}\equiv(p,\mathbf{S})\equiv(p,\mathbf{B},\mathbf{T}_{\parallel})$ where the index $\mathbf{B}$ labels the finite basis of lattice sites of the pth principal layer and $\mathbf{T}_{\parallel}$ denotes a 2D translation vector such that $\mathbf{S}=\mathbf{B}+\mathbf{T}_{\parallel}$. The lattice Fourier transform of the average GF matrix $\bar{g}(z)$ is then defined as

$$\bar{g}^{LL'}_{p\mathbf{B},p'\mathbf{B}'}(\mathbf{k}_{\parallel},z) = \sum_{\mathbf{T}_{\parallel}}\exp(i\mathbf{k}_{\parallel}\cdot\mathbf{T}_{\parallel})\bar{g}^{LL'}_{p\mathbf{B},p'(\mathbf{B}'+\mathbf{T}_{\parallel})}(z), \quad (10)$$

where $\mathbf{k}_{\parallel}$ is a vector from the 2D Brillouin zone (BZ); the transforms of other matrix quantities $[S,\mathcal{B}_{\mathcal{L}},\mathcal{B}_{\mathcal{R}},\mathcal{G}_{\mathcal{L}}(z),\mathcal{G}_{\mathcal{R}}(z)]$ are defined analogously. Employing the transformed quantities, the coherent part of the conductance, Eq. (8) is expressed as a BZ average

$$C_{\mathrm{coh}} = \frac{e^2}{h}\frac{1}{N_{\parallel}}\sum_{\mathbf{k}_{\parallel}}\mathrm{tr}\{\bar{g}(\mathbf{k}_{\parallel},a)\mathcal{B}_{\mathcal{L}}(\mathbf{k}_{\parallel})\bar{g}(\mathbf{k}_{\parallel},b)\mathcal{B}_{\mathcal{R}}(\mathbf{k}_{\parallel})\}, \quad (11)$$

where tr denotes the trace taken over the composed $(p\mathbf{B}L)$ matrix index.

The formulation and evaluation of the vertex part of the conductance, Eq. (9), requires a number of auxiliary quantities, the most important of them being the composed matrix index $\Lambda\equiv(L,L')$, site-diagonal quantities $\lambda_{\mathbf{R}}(a,b)$ with matrix elements $\lambda^{\Lambda_1\Lambda_2}_{\mathbf{R}}(a,b)$ and a matrix $\Delta(a,b)$ with elements $\Delta^{\Lambda_1\Lambda_2}_{\mathbf{R}_1\mathbf{R}_2}(a,b)$, see the Appendix. The final expression for the vertex part of the conductance is given by

$$C_{\mathrm{VC}} = \frac{e^2}{h}\sum_{p_1\mathbf{B}_1\Lambda_1}\sum_{p_2\mathbf{B}_2\Lambda_2}[\bar{g}(b)\mathcal{B}_{\mathcal{R}}\bar{g}(a)]^{\tilde{\Lambda}_1}_{p_1\mathbf{B}_1}[\Delta^{-1}(\mathbf{0}_{\parallel},a,b)]^{\Lambda_1\Lambda_2}_{p_1\mathbf{B}_1,p_2\mathbf{B}_2} \times[\bar{g}(a)\mathcal{B}_{\mathcal{L}}\bar{g}(b)]^{\Lambda_2}_{p_2\mathbf{B}_2}, \quad (12)$$

where $\tilde{\Lambda}_1\equiv(L_1',L_1)$ denotes the transposed index to $\Lambda_1\equiv(L_1,L_1')$ and the matrix elements on the right-hand side (rhs) are expressed in terms of lattice Fourier transforms,

$$[\bar{g}(a)\mathcal{B}_{\mathcal{L}}\bar{g}(b)]^{\Lambda}_{p\mathbf{B}} = \frac{1}{N_{\parallel}}\sum_{\mathbf{k}_{\parallel}}\sum_{L_1\mathbf{B}_1}\sum_{L_2\mathbf{B}_2}\bar{g}^{LL_1}_{p\mathbf{B},1\mathbf{B}_1}(\mathbf{k}_{\parallel},a) \times(\mathcal{B}_{\mathcal{L}})^{L_1L_2}_{1\mathbf{B}_1,1\mathbf{B}_2}(\mathbf{k}_{\parallel})\bar{g}^{L_2L'}_{1\mathbf{B}_2,p\mathbf{B}}(\mathbf{k}_{\parallel},b), \quad (13)$$

the definition of $[\bar{g}(b)\mathcal{B}_{\mathcal{R}}\bar{g}(a)]^{\Lambda}_{p\mathbf{B}}$ is analogous, see Eq. (A7), and

$$[\Delta(\mathbf{0}_{\parallel},a,b)]^{\Lambda_1\Lambda_2}_{p_1\mathbf{B}_1,p_2\mathbf{B}_2} = \sum_{\mathbf{T}_{\parallel}}\Delta^{\Lambda_1\Lambda_2}_{p_1\mathbf{B}_1,p_2(\mathbf{B}_2+\mathbf{T}_{\parallel})}(a,b) = \delta_{p_1p_2}\delta_{\mathbf{B}_1\mathbf{B}_2}[\lambda^{-1}_{p_1\mathbf{B}_1}(a,b)]^{\Lambda_1\Lambda_2} - \frac{1}{N_{\parallel}}\sum_{\mathbf{k}_{\parallel}}\bar{g}^{L_1L_2}_{p_1\mathbf{B}_1,p_2\mathbf{B}_2}(\mathbf{k}_{\parallel},a)\bar{g}^{L_2'L_1'}_{p_2\mathbf{B}_2,p_1\mathbf{B}_1}(\mathbf{k}_{\parallel},b). \quad (14)$$

Note that the last expression is nothing but the lattice Fourier transform for zero $\mathbf{k}_{\parallel}$ vector of the matrix $\Delta^{\Lambda_1\Lambda_2}_{\mathbf{R}_1\mathbf{R}_2}(a,b)$, Eq. (A13).

III. IMPLEMENTATION AND DETAILS OF CALCULATIONS

A. Self-consistent electronic structure

The self-consistent electronic structures were obtained using an all-electron scalar-relativistic version of the TB-LMTO-ASA method[37] within the local spin-density approximation[42] (LSDA) to the density functional theory.[43] The local exchange-correlation potential of Ref. 44 was employed and the valence basis consisted of s, p, and d orbitals. The potential functions $P_{\mathbf{R}\ell}(z)$ were parametrized with a second-order accuracy[37] and the self-consistency of one-electron potentials was achieved in intermediate regions comprising also a few monolayers (ML) of the attached metallic leads. The electrostatic dipole-barrier effects due to the dipole moments of electron densities inside the atomic spheres, non-

negligible especially at the interfaces, were included in the one-electron potentials.[37,45] The systems addressed in Sec. IV were based on face-centered-cubic (fcc) and body-centered-cubic (bcc) lattices with layers perpendicular to low-index directions and with all lattice relaxations neglected. One principal layer was formed by one atomic layer for fcc(111) stacking while two neighboring atomic layers per principal layer were necessary in fcc(001) and bcc(001) cases. The integrations over the 2D BZ were performed on a uniform mesh of about 1000 $\mathbf{k}_\parallel$ points; energy integrations over the occupied part of the valence bands were performed in the complex energy plane along a closed contour starting and ending at the Fermi energy. Further details of the numerical implementation can be found elsewhere.[37,38]

B. CPP conductances

An efficient evaluation of the conductance according to Eqs. (11)–(14) rests on a fast numerical algorithm to obtain the averaged GF matrix $\bar{g}(\mathbf{k}_\parallel,z)\equiv\{\bar{g}^{LL'}_{p\mathbf{B},p'\mathbf{B}'}(\mathbf{k}_\parallel,z)\}$ inside the intermediate region ($1\leqslant p,p'\leqslant N$). This matrix is defined as the inverse of a block-tridiagonal matrix (with vanishing blocks for $|p-p'|>1$).[10,37,38] In particular, the coherent part of the conductance, Eq. (11), requires only two corner blocks of $\bar{g}(\mathbf{k}_\parallel,z)$, namely for $p=1$, $p'=N$ and $p=N$, $p'=1$, and an order-N technique can be used for this purpose.[46]

The evaluation of the vertex part of the conductance is more demanding mainly because all blocks of $\bar{g}(\mathbf{k}_\parallel,z)$ enter Eqs. (12)–(14) and the procedure becomes roughly of order-N^2.[46] A more careful analysis reveals that the VC $\Gamma^{\Lambda}_{\mathbf{R}}(a,b)$ are nonvanishing only for sites with true randomness, see Eq. (A8). Moreover, the range of indices p and $\mathbf{B}$ in Eqs. (12)–(14) must be limited to such sites in order to keep the matrix $\Delta(\mathbf{0}_\parallel,a,b)$ well defined. Its inversion requires at most order-N^3 operations, but it does not lead to a significant increase of computing time in practice since this inversion must be done only once during the whole calculation. A faster approach (essentially of order-N) can be developed for systems with disorder limited to a finite (N-indepenent) number of layers but this route has not been followed here.

The imaginary parts of energy arguments a and b for conductance calculations were taken $\pm 10^{-7}$ Ry while the BZ averages were evaluated using $N_\parallel\approx 3000$ $\mathbf{k}_\parallel$ points. The point group symmetry of individual systems was taken into account so that only the irreducible parts of the 2D BZ were sampled, reducing thus computation times and memory requirements. The surface GF's, $\mathcal{G}_{\mathcal{R}}(z)$ and $\mathcal{G}_{\mathcal{L}}(z)$ for $z=a,b$, were calculated by employing the renormalization-decimation technique.[37,47] The potential functions at the Fermi energy were obtained from the second-order parametrization again[29] while the corresponding coherent potential functions $\mathcal{P}^{LL'}_{\mathbf{R}}(z)$ (for $z=a,b$) were obtained first by solving the CPA self-consistency condition, Eq. (3), outside the real energy axis and then by a numerical analytic continuation to the real axis.[48]

The calculated conductances using the CPA were in several cases compared to results of a SC approach.[10,12,32] The latter was based on site- and species-dependent potential functions $P^{Q}_{\mathbf{R}\ell}(z)$ obtained from LSDA-CPA self-consistent calculations. The substitutional disorder was simulated by 5×5 lateral supercells in individual atomic layers, with random occupations of the sites produced by a random-number generator (with constraints imposed by given layer-resolved alloy concentrations). The conductances resulted from a uniform sampling of the 2D BZ of the SC by 400 $\mathbf{k}_\parallel$ points.

TABLE I. Spin-resolved CPP conductances (in e^2/h per interface atom) for fcc(001) 5 ML Co-4 ML Cu-5 ML Co trilayers sandwiched by two Cu leads in FM and AF arrangements and the MR-ratio γ. The rough interfaces were simulated with the concentration variable $x=0.16$ (see text for details).

Interfaces	$C^{\uparrow}_{\mathrm{FM}}$	$C^{\downarrow}_{\mathrm{FM}}$	$C^{\uparrow\downarrow}_{\mathrm{AF}}$	γ
Ideal	0.743	0.238	0.228	1.15
Rough (SC)	0.733	0.256	0.354	0.40
Rough (CPA)	0.722	0.260	0.356	0.38
Rough (CPA, coherent)	0.673	0.016	0.054	5.38

IV. RESULTS

The total conductances of the systems studied below are given by sums over the two spin channels, $C=C^{\uparrow}+C^{\downarrow}$, where the spin-resolved conductances C^{σ} were calculated separately according to Sec. III B. For systems containing two magnetic layers adjacent to a nonmagnetic spacer, two magnetic arrangements were considered, namely the ferromagnetic (FM) and the antiferromagnetic (AF) one, and a magnetoresistance (MR) ratio was defined in terms of the corresponding conductances C_{FM}, C_{AF} as

$$\gamma=\frac{C_{\mathrm{FM}}}{C_{\mathrm{AF}}}-1. \tag{15}$$

A. Rough interfaces in Co-Cu-Co trilayers

The effects of interface intermixing on the CPP conductances in Co/Cu-based epitaxial systems have been investigated in a number of recent papers.[10–12,16,49] Here we studied fcc(001) 5 ML Co-4 ML Cu-5 ML Co trilayers sandwiched by two semi-infinite Cu leads with all four interfaces imperfect; the atoms were placed at sites of an ideal Co fcc lattice (with a lattice parameter smaller by $\sim 2\%$ than that of pure Cu). The interface roughness was simulated by disordered alloys in two atomic layers at each Co/Cu interface; the neighboring layers have composition $\mathrm{Co}_{1-x}\mathrm{Cu}_x$ on the Co side and $\mathrm{Co}_x\mathrm{Cu}_{1-x}$ on the Cu side, where x is a concentration variable, $0\leqslant x\leqslant 0.5$. As noted in Ref. 12, the particular thicknesses of the Co and Cu layers are less important for understanding the influence of disorder on the CPP magnetotransport in this model.

Table I compares the CPA results with those of the SC technique for $x=0.16$;[12] the coherent parts of the CPA conductances and results for ideal interfaces ($x=0$) are listed as well. Note that the AF conductances for the two spin channels coincide due to the geometric symmetry of the trilayers.

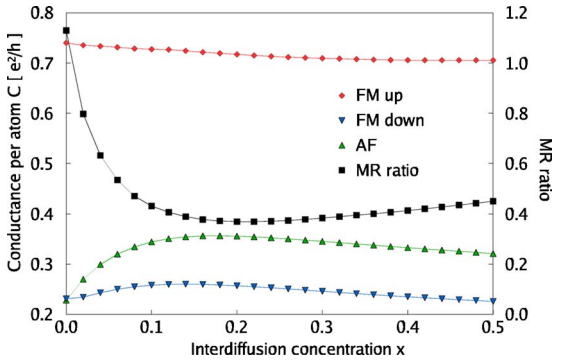

FIG. 1. (Color online) Spin-resolved CPP conductances in FM and AF arrangements and the MR ratio for fcc(001) 5 ML Co-4 ML Cu-5 ML Co trilayers sandwiched by two Cu leads as functions of the concentration x of interdiffused atoms at the rough interfaces.

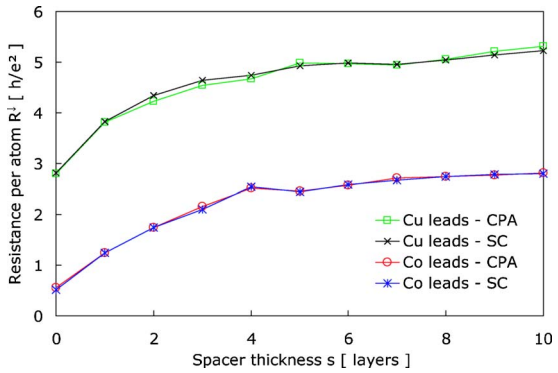

FIG. 2. (Color online) Resistances per one interface atom of the fcc(001) 5 ML Co-s ML $Cu_{0.84}Ni_{0.16}$-5 ML Co trilayers sandwiched by two pure fcc(001) Cu and Co leads for minority electrons and the FM orientation of the Co slabs. The present CPA values are compared to the SC results of Ref. 12.

The data in Table I indicate several important facts. First, the good agreement between the SC and CPA results indicates that the CPA—being an effective-medium theory—is reliable even for 2D alloys, in contrast to common wisdom on a general failure of mean-field-like approaches in low-dimensional structures. The present case, however, is not a genuine 2D system; the imaginary parts of self-energies of the (nonrandom) metallic leads play a significant role for the success of the CPA. Second, the non-negligible deviations of the coherent CPA conductances with respect to the total conductances prove the importance of the VC. Third, a comparison to results for the trilayer with ideal interfaces reveals a strong sensitivity of the MR ratio to the interface roughness. The last two conclusions have already been done using the SC approach.[12]

The concentration dependence of the transport quantities is depicted in Fig. 1. One can observe a nearly constant spin-↑ FM conductance that decreases only very weakly with increasing x, accompanied by nonmonotonous dependences of conductances in spin-↓ FM and spin-↑↓ AF channels. The strong increase of the AF conductance for small values of x is entirely due to the incoherent part (cf. Table I), that is equivalent to opening of new conductance channels as obtained from the previous SC approach.[10,12] A similar but weaker concentration dependence is seen in the spin-↓ FM channel; the resulting MR-ratio γ exhibits a rapid decrease from a value of 115% for ideal interfaces down to a minimum $\gamma_{\min} \approx 37\%$ around $x \approx 0.2$ followed by a very slow increase up to 45% at $x=0.5$ (Fig. 1). This strong sensitivity of MR ratio to small amount of interface disorder contradicts a recent prediction of minor GMR changes due to the rough interfaces.[16] Note however that the SC calculations of Ref. 16 were performed only for a single Co/Cu(001) interface while the present model contains four intermixed interfaces; the MR ratio decreases with increasing number of rough Co/Cu interfaces, as shown in another SC study.[10] Reflection and transmission probabilities and specularity parameters of a single rough Co/Cu(001) interface have recently been investigated using a LKKR-CPA approach.[49] In agreement with the present results, the calculated probabilities of Ref. 49 exhibit pronounced changes due to a small ($x \sim 0.1$) amount of disorder; however the underlying $\mathbf{k}_\parallel$-resolved quantities are based on a highly simplified form of the VC and their reliability for a thorough quantitative analysis is thus limited.

B. Random nonmagnetic spacer in Co-CuNi-Co trilayers

The effect of random Ni impurities in the Cu spacer on the CPP transport in fcc(001) Co-Cu-Co trilayers has been studied in details by the SC technique.[12] For this reason we focus here merely on a comparison of the present CPA results to the existing SC values for two cases, namely for fcc(001) 5 ML Co-s ML $Cu_{0.84}Ni_{0.16}$-5 ML Co trilayers sandwiched by two pure fcc(001) Cu and Co leads. Note that the latter case refers to the CuNi slab embedded between two semi-infinite Co leads. We have taken the ideal fcc Co lattice in both cases (see Sec. IV A) and considered the minority spin ($\sigma = \downarrow$) channel of the FM arrangement with the CuNi spacer thickness s varying in the range $1 \leqslant s \leqslant 10$.

The results are plotted as resistances $R^{\downarrow}_{\mathrm{FM}}(s) = 1/C^{\downarrow}_{\mathrm{FM}}(s)$ in Fig. 2. The depicted resistances prove a very good quantitative agreement between the two approaches (CPA, SC) for both leads (Cu, Co); in particular, the different slopes of $R^{\downarrow}_{\mathrm{FM}}(s)$ for very thin spacers as compared to thicker spacers are clearly reproduced. This phenomenon can be explained by quantum-well states formed in Cu-based spacers sandwiched by two Co slabs.[12,50] The degree of agreement shown in Fig. 2 indicates that the localized nature of the quantum-well states does not represent a principal obstacle for applicability of the CPA.

C. Random magnetic layer in CoCr-Cu-Co trilayers

Recently, several various F1-Cu-Co-Cu fcc(111) multilayers containing a random binary ferromagnetic alloy F1 have been manufactured that exhibit a transition from a positive to negative GMR effect with increasing thickness M of the ferromagnetic alloy.[31] The value of M where the transition occurs is called a compensation thickness. The experimental observation has been explained theoretically for $Co_{0.8}Cr_{0.2}$-Cu-Co trilayers using the SC method.[32] The origin of the negative GMR was identified with a ferrimagnetic spin struc-

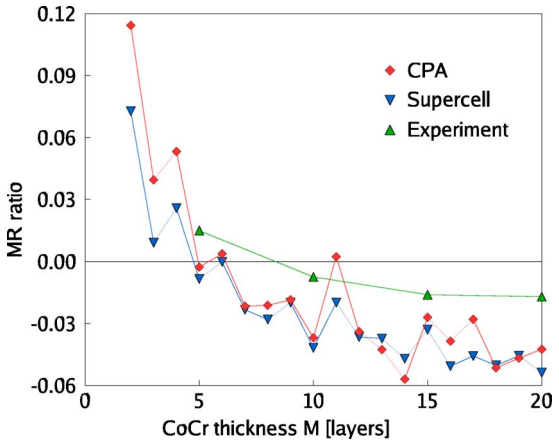

FIG. 3. (Color online) MR ratio for fcc(111) trilayers M ML $Co_{0.8}Cr_{0.2}$-20 ML Cu-2 ML Co sandwiched by two Cu leads calculated by the present CPA approach and the SC technique of Ref. 32 as functions of the CoCr slab thickness M. The experimental values of Ref. 31 refer to $Co_{0.8}Cr_{0.2}$-Cu-Co-Cu multilayers.

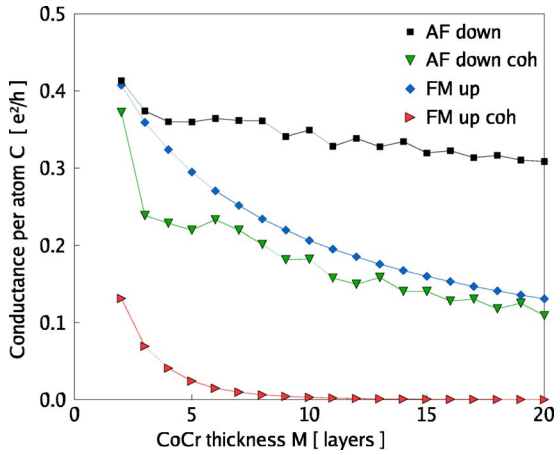

FIG. 4. (Color online) CPP conductances of fcc(111) trilayers M ML $Co_{0.8}Cr_{0.2}$-20 ML Cu-2 ML Co sandwiched by two Cu leads: for spin-↑ in the FM arrangement and for spin-↓ in the AF arrangement. Both conductances are plotted together with their coherent parts.

ture of the bulk random fcc $Co_{0.8}Cr_{0.2}$ alloy that results in formation of a virtual bound state in the Cr-projected density of states of majority electrons ($\sigma = \uparrow$) of the CoCr alloy. This state reflects a strong scattering regime leading thus to a rapid decrease of the majority-spin conductances with increasing CoCr layer thickness M.

Here the CPA technique is compared to the SC approach[32] for fcc(111) trilayers M ML $Co_{0.8}Cr_{0.2}$-20 ML Cu-2 ML Co, where the CoCr layer thickness covers an interval $2 \leqslant M \leqslant 20$, sandwiched by two semi-infinite Cu leads (all atoms placed on the ideal fcc Co lattice). The resulting MR ratio of both techniques together with experimental results of Ref. 31 are shown in Fig. 3 as functions of the CoCr thickness M. The theoretical dependences exhibit very similar features, namely small oscillations on top of slowly decreasing trends; the latter follow roughly the experimentally observed dependence. The theoretical compensation thickness is around 5 ML CoCr while the experimental compensation takes place at about 8 ML. This difference can most probably be ascribed to effects of multilayer repetitions in real samples.[32]

The oscillations in the calculated CoCr thickness dependence of the MR ratio (Fig. 3) are due to quantum oscillations in the minority-spin conductances, as documented in Fig. 4 for the AF configuration. The majority-spin conductances show a completely different thickness dependence: a faster decrease with increasing M without any sign of oscillations, see Fig. 4 for the FM arrangement. The different transport regimes in the two channels are reflected also by the coherent and diffusive contributions of the conductances: while the coherent part of the majority-spin conductance represents a smaller contribution, exponentially decaying with M, the coherent part of the minority-spin conductance survives throughout the whole range of M studied and it reflects a weak scattering regime inside the CoCr slab.

The oscillations of the MR ratio, clearly present in theoretical results, are not seen in experiment.[31] For this reason, we investigated their sensitivity to interface roughness at the two CoCr/Cu interfaces by putting one atomic layer of composition $Cu_{1-x}Co_x$ on the Cu side of the interfaces, where x is a concentration variable. Figure 5 contains the results for $x = 0.2$; very similar trends were found for other values of x in an interval $0.1 \leqslant x \leqslant 0.4$, in full analogy to the Co-Cu-Co case (Sec. IV A). The obtained changes prove a strong influence of the interface roughness on the oscillations which brings the calculated MR ratio towards a better agreement with the experiment. An explanation of this effect rests on the fact that the Co impurities in the Cu layers represent strong scatterers for minority electrons suppressing thus the quantum conductance oscillations in this channel. Note however that the compensation length is only weakly affected by the interface roughness (Figs. 3 and 5).

D. (Ga,Mn)As diluted magnetic semiconductors

Layered epitaxial systems containing the p-type diluted ferromagnetic semiconductors (Ga,Mn)As are intrinsically

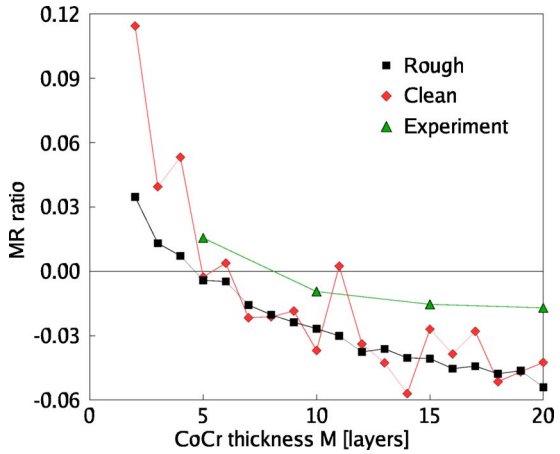

FIG. 5. (Color online) MR ratio for fcc(111) trilayers M ML $Co_{0.8}Cr_{0.2}$-20 ML Cu-2 ML Co sandwiched by two Cu leads calculated with clean and rough CoCr/Cu interfaces and compared to experimental values of Ref. 31.

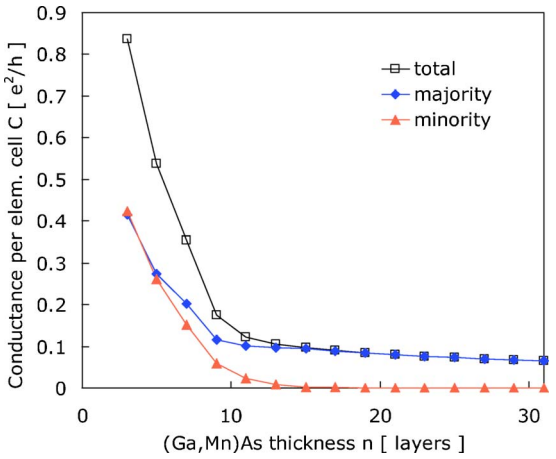

FIG. 6. (Color online) Spin-resolved CPP conductances of (Ga,Mn)As (001) slabs with 8% Mn sandwiched by two semi-infinite nonmagnetic bcc Cr(001) leads as functions of the (Ga, Mn)As thickness.

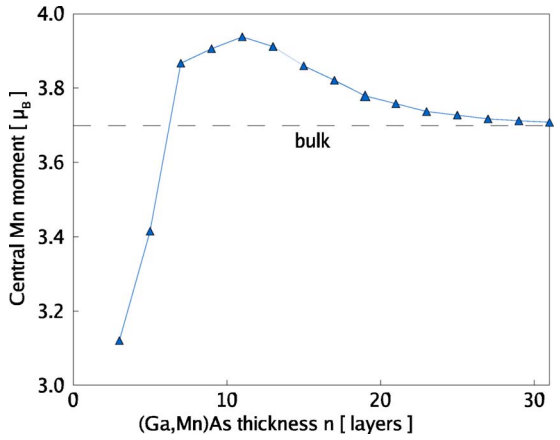

FIG. 7. (Color online) The local magnetic moment of Mn atoms in the middle of (Ga,Mn)As (001) slabs with 5% Mn sandwiched by two semi-infinite nonmagnetic bcc Cr(001) leads as a function of the slab thickness. The horizontal line marks the Mn moment in the bulk $Ga_{0.95}Mn_{0.05}As$ alloy.

disordered systems with a number of interesting transport properties.[33–35,51,52] Their detailed theory including, e.g., the role of native structural defects and effects of spin-orbit coupling, remains far beyond the scope of the present study; this section shows the first CPA results for their CPP conductances and a brief comparison to bulk residual resistivities.[30,33] The transport properties of so-called digital (Ga,Mn)As heterostructures have been studied recently;[53,54] their conductances reflect a purely ballistic regime owing to the special structures that remain nonrandom even in the presence of As antisite atoms.

The calculations reported here were performed for (001) layers of zinc-blende $Ga_{1-x}Mn_xAs$ alloys with Mn content in a range $0.05 \leqslant x \leqslant 0.08$, sandwiched by two semi-infinite bcc(001) leads of nonmagnetic chromium. Empty spheres were inserted in the tetrahedral interstitial positions of the zinc-blende structure for matters of space filling; one atomic (001) layer of the resulting bcc lattice thus contained two spheres: either a Ga sphere and an empty sphere or an As sphere and an empty sphere inside the (Ga,Mn)As slab, or two Cr spheres inside the Cr leads; all spheres have equal radii. No relaxations of an ideal bcc lattice were allowed; its lattice parameter was set according to the equilibrium fcc lattice of pure GaAs ($a=0.565$ nm) which required a small compression ($\sim 2\%$) inside the Cr leads as compared to an equilibrium bcc Cr lattice. The Mn atoms were placed randomly on the cation sublattice and the (Ga,Mn)As slabs comprised an odd number n of atomic layers, where $3 \leqslant n \leqslant 31$; the slabs were As-terminated with no disorder at the As/Cr interfaces.

The calculated total and spin-resolved CPP conductances for slabs with 8% Mn are depicted in Fig. 6. Their thickness dependence exhibits two different slopes: a rapid decrease for thin layers ($n<11$) followed by a much slower decrease for thick layers ($n>11$). The transition between these two regimes can be explained by formation of the bulklike electronic structure in the middle of thicker (Ga,Mn)As slabs; it can also be observed in the behavior of local electronic quantities as illustrated in Fig. 7 for the local spin Mn moments in the central plane of the slabs with 5% Mn. The central Mn moments in thin slabs are strongly influenced by the leads while a slow monotonous trend towards the bulk value is found only for thicker slabs. The varying influence of the Cr leads on the CPP conductances (Fig. 6) is also reflected by a weak spin polarization for $n<11$ and a strong spin polarization due to the exponentially decaying minority conductance for $n>11$. The latter feature is in agreement with the half-metallic nature of bulk defect-free (Ga,Mn)As alloys.[35,55–58]

The majority and total conductances approach an ohmic regime for thick slabs; the bulk residual resistivities[30] compare well to their counterparts derived from the CPP conductances for $n>20$, as documented in Table II. The resistivity values and their concentration dependence prove an importance of the number of carriers (holes in the valence band) in addition to the strength of impurity scattering.[30] A comparison to experimental resistivities of Ref. 33 is presented in Table II as well; the experimental values for $x=0.05$ and $x=0.06$ provide an independent check of reliability of the *ab initio* CPA scheme whereas the markedly higher resistivity measured for $x=0.08$ reflects a high amount of compensating As antisite defects in the sample.[33]

The coherent and vertex contributions to the majority conductance are shown in Fig. 8. The former decreases rapidly with (Ga,Mn)As thickness and it vanishes practically for $n>10$ whereas the latter does not change appreciably over the

TABLE II. Residual resistivities (in 10^{-5} Ω m) of $Ga_{1-x}Mn_xAs$ as obtained from the CPP conductances of thick (Ga,Mn)As(001) slabs sandwiched by two nonmagnetic bcc(001) Cr leads and from bulk calculations of Ref. 30. The experimental values are taken from Ref. 33.

Mn content x	ρ_{CPP}	ρ_{bulk}	ρ_{exp}
0.05	1.23±0.04	1.20	1.49
0.06	1.06±0.02	1.07	1.32
0.08	0.88±0.01	0.89	2.87

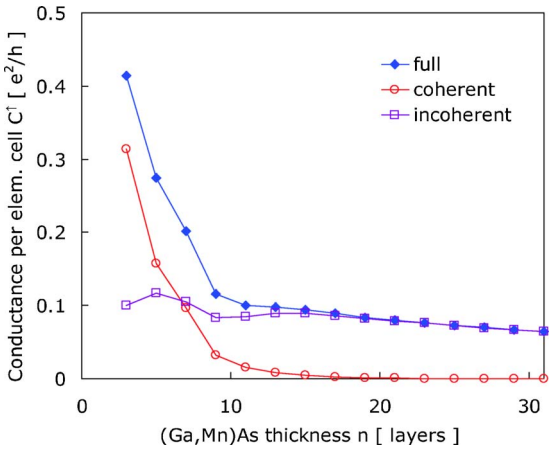

FIG. 8. (Color online) Majority-spin CPP conductance of (Ga,Mn)As (001) slabs with 8% Mn sandwiched by two semi-infinite nonmagnetic bcc Cr(001) leads together with its coherent and vertex parts.

range of n studied. These trends witness that the intrinsic disorder of (Ga,Mn)As slabs is strong enough to destroy the coherence after a very short distance traveled by electrons. This conclusion is in qualitative agreement with effects of strong disorder (nonquasiparticle behavior) manifested in the Bloch spectral function of majority electrons at the Fermi level of the bulk alloy.[59]

V. CONCLUSIONS

An *ab initio* technique for calculations of CPP transport properties of realistic epitaxial magnetic multilayers has been developed and implemented within the all-electron TB-LMTO method. It is based on a systematic use of the CPA for an efficient treatment of substitutional disorder at the interfaces and/or inside the individual layers. Its most difficult part—an evaluation of the vertex corrections—provides a natural framework for separating the coherent and incoherent contributions to the CPP conductances.

A comparison of the CPA results to those of a SC approach performed for a variety of systems confirms that important aspects of the spin-polarized CPP electron transport are fully within the reach of an effective medium treatment. The particular investigated cases include 2D randomness at rough interfaces in Co-Cu-Co trilayers, quantum-well states and randomness inside the spacer layers in Co-CuNi-Co system, and the virtual bound state in disordered magnetic layers of CoCr-Cu-Co system. A study of simultaneous randomness inside the layers and at the interfaces in the latter system revealed a pronounced sensitivity of quantum oscillations of the MR ratio and a fair stability of the compensation CoCr thickness necessary for the change of sign of the GMR effect. The first application to diluted ferromagnetic (Ga, Mn)As semiconductors yields CPP conductances compatible with calculated and measured bulk residual resistivities and with half-metallic features of the underlying electronic structure. The thickness dependence of the coherent and incoherent conductances reflects unambiguously a strong impurity scattering of majority electrons.

In summary, the developed CPA technique represents a physically sound and numerically competitive alternative to the widely used SC approaches. It can be generalized beyond the two current model by including the spin-orbit coupling and possible noncollinear magnetic configurations. This would extend the area of applicability of the CPA to other multilayers of technological interest, the only exceptions being probably systems with topological disorder (interfaces with large lattice mismatch, layers with amorphous structure).

ACKNOWLEDGMENTS

This work was supported by the Academy of Sciences of the Czech Republic (Grants Nos. AV0Z20410507, AV0Z10100520, A100100616) and the Ministry of Education of the Czech Republic (Grant No. MSM0021620834). One of the authors (O.B.) acknowledges support of CINES under Grant No. gem1100.

APPENDIX: VERTEX CORRECTIONS IN THE LMTO-CPA METHOD

This appendix contains general basic relations to derive CPA averages

$$\mathrm{Tr}\langle g(a)Bg(b)B'\rangle, \tag{A1}$$

where $g(z)$ denotes the TB-LMTO auxiliary GF matrix, a and b are two energy arguments, and B and B' are nonrandom matrices. Averages of this kind appear in transport studies and the CPP conductance, Eq. (5), represents just one example. Another particular case is the residual conductivity of random bulk alloys;[29] its full treatment for systems with multiple sublattices has been worked out recently.[30] The derivation below closely follows Ref. 23.

The starting point in handling the average (A1) is a relation

$$\langle g(a)Bg(b)\rangle = \bar{g}(a)B\bar{g}(b) + \bar{g}(a)\Gamma(a,b)\bar{g}(b), \tag{A2}$$

where the first term on the right-hand side represents the coherent contribution while the second term defines implicitly the corresponding VC. The form of the second term follows from an expansion of the GF matrix of a random configuration with respect to the averaged GF matrix

$$g(z) = \bar{g}(z) + \bar{g}(z)T(z)\bar{g}(z),$$

$$T(z) = -\sum_{\mathbf{R}} t_{\mathbf{R}}(z) + \sum_{\mathbf{R}\neq\mathbf{R}'} t_{\mathbf{R}}(z)\bar{g}(z)t_{\mathbf{R}'}(z) - \sum_{\mathbf{R}\neq\mathbf{R}'\neq\mathbf{R}''} t_{\mathbf{R}}(z)\bar{g}(z)t_{\mathbf{R}'}(z)\bar{g}(z)t_{\mathbf{R}''}(z) + \cdots, \tag{A3}$$

where $T(z)$ denotes the total T-matrix and the exclusions in summations prevent the scattering twice in sequence on the same lattice site. The random single-site T-matrix $t_{\mathbf{R}}(z)$ in Eq. (A3) must be understood as a site-diagonal matrix with elements $[t_{\mathbf{R}}(z)]^{L_1L_2}_{\mathbf{R}_1\mathbf{R}_2} = \delta_{\mathbf{R}\mathbf{R}_1}\delta_{\mathbf{R}\mathbf{R}_2}t^{Q;L_1L_2}_{\mathbf{R}}(z)$ depending on the

species Q occupying the site $\mathbf{R}$. Note that within the CPA, the self-consistency conditions, Eq. (3), are equivalent to the exact relation $\langle T(z)\rangle=0$. This allows to write down an exact expression for the VC,

$$\Gamma(a,b)=\langle T(a)\bar{g}(a)B\bar{g}(b)T(b)\rangle. \tag{A4}$$

Inserting the expansion (A3) into Eq. (A4) and using a CPA-like decoupling together with the self-consistency conditions, Eq. (3), leads to the VC as a sum of single-site contributions, $\Gamma(a,b)=\Sigma_{\mathbf{R}}\Gamma_{\mathbf{R}}(a,b)$. The contributions $\Gamma_{\mathbf{R}}(a,b)$ satisfy a set of linear equations

$$\Gamma_{\mathbf{R}}(a,b)=\langle t_{\mathbf{R}}(a)\bar{g}(a)B\bar{g}(b)t_{\mathbf{R}}(b)\rangle + \sum_{\mathbf{R}'(\neq\mathbf{R})}\langle t_{\mathbf{R}}(a)\bar{g}(a)\Gamma_{\mathbf{R}'}(a,b)\bar{g}(b)t_{\mathbf{R}}(b)\rangle, \tag{A5}$$

that define unambiguously the VC in the CPA.

The solution of Eqs. (A5) is greatly facilitated by the localized nature of the single-site T-matrices $t_{\mathbf{R}}(z)$, see text below Eq. (A3). Consequently, the site contributions $\Gamma_{\mathbf{R}}(a,b)$ are localized as well, i.e., their matrix elements are $[\Gamma_{\mathbf{R}}(a,b)]^{L_1L_2}_{\mathbf{R}_1\mathbf{R}_2}=\delta_{\mathbf{R}\mathbf{R}_1}\delta_{\mathbf{R}\mathbf{R}_2}\Gamma^{L_1L_2}_{\mathbf{R}}(a,b)$. The linear relations (A5) are then recast in terms of the matrix elements as

$$\Gamma^{L_1L_1'}_{\mathbf{R}}(a,b)=\sum_{Q}\sum_{L_2L_2'}c^{Q}_{\mathbf{R}}t^{Q;L_1L_2}_{\mathbf{R}}(a)[\bar{g}(a)B\bar{g}(b)]^{L_2L_2'}_{\mathbf{R}\mathbf{R}}t^{Q;L_2'L_1'}_{\mathbf{R}}(b) + \sum_{Q}\sum_{\mathbf{R}'(\neq\mathbf{R})}\sum_{L_2L_2'}\sum_{L_3L_3'}c^{Q}_{\mathbf{R}}t^{Q;L_1L_2}_{\mathbf{R}}(a)\bar{g}^{L_2L_3}_{\mathbf{R}\mathbf{R}'}(a) \times\Gamma^{L_3L_3'}_{\mathbf{R}'}(a,b)\bar{g}^{L_3'L_2'}_{\mathbf{R}'\mathbf{R}}(b)t^{Q;L_2'L_1'}_{\mathbf{R}}(b). \tag{A6}$$

They can be formally simplified by introducing composed indices $\Lambda\equiv(L,L')$, $\Lambda_1\equiv(L_1,L_1')$, etc., and following auxiliary variables:

$$\Gamma^{\Lambda}_{\mathbf{R}}(a,b)=\Gamma^{LL'}_{\mathbf{R}}(a,b),$$

$$\zeta^{\Lambda}_{\mathbf{R}}(a,b)=[\bar{g}(a)B\bar{g}(b)]^{LL'}_{\mathbf{R}\mathbf{R}}=[\bar{g}(a)B\bar{g}(b)]^{\Lambda}_{\mathbf{R}},$$

$$w^{\Lambda_1\Lambda_2}_{\mathbf{R}}(a,b)=\sum_{Q}c^{Q}_{\mathbf{R}}t^{Q;L_1L_2}_{\mathbf{R}}(a)t^{Q;L_2'L_1'}_{\mathbf{R}}(b),$$

$$\chi^{\Lambda_1\Lambda_2}_{\mathbf{R}\mathbf{R}'}(a,b)=(1-\delta_{\mathbf{R}\mathbf{R}'})\bar{g}^{L_1L_2}_{\mathbf{R}\mathbf{R}'}(a)\bar{g}^{L_2'L_1'}_{\mathbf{R}'\mathbf{R}}(b). \tag{A7}$$

The original Eqs. (A6) can then be rewritten compactly as

$$\Gamma^{\Lambda_1}_{\mathbf{R}}=\sum_{\Lambda_2}w^{\Lambda_1\Lambda_2}_{\mathbf{R}}\zeta^{\Lambda_2}_{\mathbf{R}}+\sum_{\mathbf{R}';\Lambda_2\Lambda_3}w^{\Lambda_1\Lambda_2}_{\mathbf{R}}\chi^{\Lambda_2\Lambda_3}_{\mathbf{R}\mathbf{R}'}\Gamma^{\Lambda_3}_{\mathbf{R}'}, \tag{A8}$$

where energy arguments (a,b) of all quantities have been omitted for brevity. The solution of this set of linear equations for $\Gamma^{\Lambda}_{\mathbf{R}}$ can be expressed using a matrix inversion

$$\Gamma=(1-w\chi)^{-1}w\zeta=(w^{-1}-\chi)^{-1}\zeta, \tag{A9}$$

where the composed matrix indices $(\mathbf{R},\Lambda)$ were suppressed and where w denotes a site-diagonal matrix with elements $w^{\Lambda_1\Lambda_2}_{\mathbf{R}\mathbf{R}'}(a,b)=\delta_{\mathbf{R}\mathbf{R}'}w^{\Lambda_1\Lambda_2}_{\mathbf{R}}(a,b)$.

The solution for the vertex corrections (A9) can be given another form more suitable for direct calculations. A definition of a matrix quantity $\psi_{\mathbf{R}\mathbf{R}'}(a,b)$ and of its site-diagonal blocks $\varphi_{\mathbf{R}}(a,b)\equiv\psi_{\mathbf{R}\mathbf{R}}(a,b)$ given by

$$\psi^{\Lambda_1\Lambda_2}_{\mathbf{R}\mathbf{R}'}(a,b)=\bar{g}^{L_1L_2}_{\mathbf{R}\mathbf{R}'}(a)\bar{g}^{L_2'L_1'}_{\mathbf{R}'\mathbf{R}}(b),$$

$$\varphi^{\Lambda_1\Lambda_2}_{\mathbf{R}}(a,b)=\bar{g}^{L_1L_2}_{\mathbf{R}\mathbf{R}}(a)\bar{g}^{L_2'L_1'}_{\mathbf{R}\mathbf{R}}(b), \tag{A10}$$

leads to a trivial relation $\psi_{\mathbf{R}\mathbf{R}'}(a,b)=\delta_{\mathbf{R}\mathbf{R}'}\varphi_{\mathbf{R}}(a,b)+\chi_{\mathbf{R}\mathbf{R}'}(a,b)$ and to the complete vertex operators[23] represented by site-diagonal quantities $\lambda^{\Lambda_1\Lambda_2}_{\mathbf{R}}(a,b)$ defined by

$$\lambda^{-1}_{\mathbf{R}}(a,b)=w^{-1}_{\mathbf{R}}(a,b)+\varphi_{\mathbf{R}}(a,b). \tag{A11}$$

The vertex corrections can be now reformulated as

$$\Gamma=\Delta^{-1}\zeta,\quad \Delta=\lambda^{-1}-\psi, \tag{A12}$$

or, with all matrix indices and energy arguments restored,

$$\Gamma^{\Lambda_1}_{\mathbf{R}_1}(a,b)=\sum_{\mathbf{R}_2\Lambda_2}[\Delta^{-1}(a,b)]^{\Lambda_1\Lambda_2}_{\mathbf{R}_1\mathbf{R}_2}\zeta^{\Lambda_2}_{\mathbf{R}_2}(a,b),$$

$$\Delta^{\Lambda_1\Lambda_2}_{\mathbf{R}_1\mathbf{R}_2}(a,b)=\delta_{\mathbf{R}_1\mathbf{R}_2}[\lambda^{-1}_{\mathbf{R}_1}(a,b)]^{\Lambda_1\Lambda_2}-\psi^{\Lambda_1\Lambda_2}_{\mathbf{R}_1\mathbf{R}_2}(a,b). \tag{A13}$$

The advantage of the last expression is due to the fact that λ is site-diagonal and ψ has a simpler structure than χ. Using the (two- or three-dimensional) translational invariance of the configurationally averaged system, the matrix inversion in Eq. (A13) can easily be performed in terms of lattice Fourier transforms of the quantities involved.[23] The solution is very simple for operators B exhibiting the same translational invariance since it requires the Fourier transform of the matrix $\Delta^{\Lambda_1\Lambda_2}_{\mathbf{R}_1\mathbf{R}_2}(a,b)$ only for zero $\mathbf{k}$ vector in the reciprocal space.[24]

Finally, the average (A1) can be decomposed into the coherent and the incoherent (vertex) part, as based on Eq. (A2),

$$\mathrm{Tr}\langle g(a)Bg(b)B'\rangle=\mathrm{Tr}\{\bar{g}(a)B\bar{g}(b)B'\}+\mathrm{Tr}\langle g(a)Bg(b)B'\rangle_{\mathrm{VC}}. \tag{A14}$$

An explicit expression for the vertex contribution is obtained from Eq. (A13),

$$\begin{aligned}\mathrm{Tr}\langle g(a)Bg(b)B'\rangle_{\mathrm{VC}} &=\mathrm{Tr}\{\bar{g}(a)\Gamma(a,b)\bar{g}(b)B'\}\\ &=\sum_{\mathbf{R}_1\Lambda_1}\sum_{\mathbf{R}_2\Lambda_2}[\bar{g}(b)B'\bar{g}(a)]^{\tilde{\Lambda}_1}_{\mathbf{R}_1}[\Delta^{-1}(a,b)]^{\Lambda_1\Lambda_2}_{\mathbf{R}_1\mathbf{R}_2}[\bar{g}(a)B\bar{g}(b)]^{\Lambda_2}_{\mathbf{R}_2},\end{aligned} \tag{A15}$$

where $[\bar{g}(b)B'\bar{g}(a)]^{\tilde{\Lambda}_1}_{\mathbf{R}_1}$ is defined similarly to Eq. (A7) with $\tilde{\Lambda}_1\equiv(L'_1,L_1)$ denoting the transpose of $\Lambda_1\equiv(L_1,L'_1)$.

*Electronic address: carva@karlov.mff.cuni.cz

[1] M. N. Baibich J. M. Broto, A. Fert, F. Nguyen Van Dau, F. Petroff, P. Eitenne, G. Creuzet, A. Friederich, and J. Chazelas, Phys. Rev. Lett. **61**, 2472 (1988).
[2] G. Binasch, P. Grünberg, F. Saurenbach, and W. Zinn, Phys. Rev. B **39**, 4828 (1989).
[3] J. Bass and W. P. Pratt, Jr., J. Magn. Magn. Mater. **200**, 274 (1999).
[4] *Spin Dependent Transport in Magnetic Nanostructures*, edited by S. Maekawa and T. Shinjo (CRC, Boca Raton, FL, 2002).
[5] P. Weinberger, Phys. Rep. **377**, 281 (2003).
[6] R. Coehoorn, in *Handbook of Magnetic Materials*, edited by K. H. J. Buschow (North-Holland, Amsterdam, 2003), Vol. 15, Chap. 1, p. 1.
[7] S. Datta, *Electronic Transport in Mesoscopic Systems* (Cambridge University Press, Cambridge, 1995).
[8] D. Wortmann, H. Ishida, and S. Blügel, Phys. Rev. B **65**, 165103 (2002).
[9] D. Wortmann, H. Ishida, and S. Blügel, Phys. Rev. B **66**, 075113 (2002).
[10] J. Kudrnovský, V. Drchal, C. Blaas, P. Weinberger, I. Turek, and P. Bruno, Phys. Rev. B **62**, 15084 (2000).
[11] K. Xia, P. J. Kelly, G. E. W. Bauer, I. Turek, J. Kudrnovský, and V. Drchal, Phys. Rev. B **63**, 064407 (2001).
[12] V. Drchal, J. Kudrnovský, P. Bruno, P. H. Dederichs, I. Turek, and P. Weinberger, Phys. Rev. B **65**, 214414 (2002).
[13] P. Mavropoulos, N. Papanikolaou, and P. H. Dederichs, Phys. Rev. B **69**, 125104 (2004).
[14] P. Weinberger, P. M. Levy, J. Banhart, L. Szunyogh, and B. Újfalussy, J. Phys.: Condens. Matter **8**, 7677 (1996).
[15] J. M. MacLaren, X.-G. Zhang, W. H. Butler, and X. Wang, Phys. Rev. B **59**, 5470 (1999).
[16] J. Velev and W. H. Butler, Phys. Rev. B **69**, 024404 (2004).
[17] P. Soven, Phys. Rev. **156**, 809 (1967).
[18] B. Velický, S. Kirkpatrick, and H. Ehrenreich, Phys. Rev. **175**, 747 (1968).
[19] R. J. Elliott, J. A. Krumhansl, and P. L. Leath, Rev. Mod. Phys. **46**, 465 (1974).
[20] H. Itoh, J. Inoue, A. Umerski, and J. Mathon, Phys. Rev. B **68**, 174421 (2003).
[21] E. Y. Tsymbal and D. G. Pettifor, Phys. Rev. B **54**, 15314 (1996).
[22] R. Kubo, J. Phys. Soc. Jpn. **12**, 570 (1957).
[23] B. Velický, Phys. Rev. **184**, 614 (1969).
[24] W. H. Butler, Phys. Rev. B **31**, 3260 (1985).
[25] J. C. Swihart, W. H. Butler, G. M. Stocks, D. M. Nicholson, and R. C. Ward, Phys. Rev. Lett. **57**, 1181 (1986).
[26] H. Ebert, A. Vernes, and J. Banhart, Phys. Rev. B **54**, 8479 (1996).
[27] J. Banhart and G. Czycholl, Europhys. Lett. **58**, 264 (2002).
[28] L. Dulca, J. Banhart, and G. Czycholl, Phys. Rev. B **61**, 16502 (2000).
[29] I. Turek, J. Kudrnovský, V. Drchal, L. Szunyogh, and P. Weinberger, Phys. Rev. B **65**, 125101 (2002).
[30] I. Turek, J. Kudrnovský, V. Drchal, and P. Weinberger, J. Phys.: Condens. Matter **16**, S5607 (2004).
[31] C. Vouille, A. Barthélémy, F. Elokan Mpondo, A. Fert, P. A. Schroeder, S. Y. Hsu, A. Reilly, and R. Loloee, Phys. Rev. B **60**, 6710 (1999).
[32] O. Bengone, O. Eriksson, S. Mirbt, I. Turek, J. Kudrnovský, and V. Drchal, Phys. Rev. B **69**, 092406 (2004).
[33] K. W. Edmonds *et al.*, Appl. Phys. Lett. **81**, 4991 (2002).
[34] D. Chiba, F. Matsukura, and H. Ohno, Physica E (Amsterdam) **21**, 966 (2004).
[35] F. Matsukura, H. Ohno, and T. Dietl, in *Handbook of Magnetic Materials*, edited by K. H. J. Buschow (North-Holland, Amsterdam, 2002), Vol. 14, Chap. 1, p. 1.
[36] O. K. Andersen and O. Jepsen, Phys. Rev. Lett. **53**, 2571 (1984).
[37] I. Turek, V. Drchal, J. Kudrnovský, M. Šob, and P. Weinberger, *Electronic Structure of Disordered Alloys, Surfaces and Interfaces* (Kluwer, Boston, 1997).
[38] I. Turek, J. Kudrnovský, and V. Drchal, in *Electronic Structure and Physical Properties of Solids*, edited by H. Dreyssé, Lecture Notes in Physics, Vol. 535 (Springer, Berlin, 2000), p. 349.
[39] O. Gunnarsson, O. Jepsen, and O. K. Andersen, Phys. Rev. B **27**, 7144 (1983).
[40] J. Kudrnovský and V. Drchal, Phys. Rev. B **41**, 7515 (1990).
[41] B. Wenzien, J. Kudrnovský, V. Drchal, and M. Šob, J. Phys.: Condens. Matter **1**, 9893 (1989).
[42] U. von Barth and L. Hedin, J. Phys. C **5**, 1629 (1972).
[43] P. Hohenberg and W. Kohn, Phys. Rev. **136**, B864 (1964).
[44] S. H. Vosko, L. Wilk, and M. Nusair, Can. J. Phys. **58**, 1200 (1980).
[45] H. L. Skriver and N. M. Rosengaard, Phys. Rev. B **43**, 9538 (1991).
[46] E. M. Godfrin, J. Phys.: Condens. Matter **3**, 7843 (1991).
[47] M. P. López Sancho, J. M. López Sancho, and J. Rubio, J. Phys. F: Met. Phys. **15**, 851 (1985).
[48] K. C. Hass, B. Velický, and H. Ehrenreich, Phys. Rev. B **29**, 3697 (1984).
[49] D. A. Stewart, W. H. Butler, X.-G. Zhang, and V. F. Los, Phys. Rev. B **68**, 014433 (2003).
[50] E. Y. Tsymbal and D. G. Pettifor, Phys. Rev. B **61**, 506 (2000).
[51] H. Ohno, J. Magn. Magn. Mater. **200**, 110 (1999).
[52] D. Chiba, Y. Sato, T. Kita, F. Matsukura, and H. Ohno, Phys. Rev. Lett. **93**, 216602 (2004).
[53] S. Sanvito and N. A. Hill, Phys. Rev. Lett. **87**, 267202 (2001).
[54] S. Sanvito, Phys. Rev. B **68**, 054425 (2003).
[55] H. Akai, Phys. Rev. Lett. **81**, 3002 (1998).
[56] S. Sanvito, P. Ordejón, and N. A. Hill, Phys. Rev. B **63**, 165206 (2001).
[57] F. Máca and J. Mašek, Phys. Rev. B **65**, 235209 (2002).
[58] J. Kudrnovský, I. Turek, V. Drchal, F. Máca, P. Weinberger, and P. Bruno, Phys. Rev. B **69**, 115208 (2004).
[59] J. Kudrnovský, V. Drchal, F. Máca, I. Turek, G. Bouzerar, and P. Bruno, in *Complex Inorganic Solids—Structural, Stability, and Magnetic Properties of Alloys*, edited by P. E. A. Turchi, A. Gonis, K. Rajan, and A. Meike (Springer, New York, 2005), p. 277.